CZECH TECHNICAL UNIVERSITY IN PRAGUE

Faculty of Nuclear Sciences and Physical Engineering

Department of Physics

Research project

Investigation of the theoretical uncertainties in the jet production kinematics

Výzkum vlivu teoretických neurčitostí na kinematiku jetové produkce

Bc. Vladimir Zitka

Supervisor: Ing. Miroslav Myska, Ph.D.

Prague, 2017/18

ČESKÉ VYSOKÉ UČENÍ TECHNICKÉ V PRAZE
FAKULTA JADERNÁ A FYZIKÁLNĚ INŽENÝRSKÁ
PRAHA 1 - STARÉ MĚSTO, BŘEHOVÁ 7 - PSČ 115 19

Katedra: fyziky **Akademický rok:** 2017/2018

VÝZKUMNÝ ÚKOL

Student: **Bc. Vladimír Žitka**

Studijní program: **NMS**

Obor: **EJČF**

Vedoucí úkolu: Ing. Miroslav Myška, Ph.D.
Název úkolu (česky/anglicky): Výzkum vlivu teoretických neurčitostí na kinematiku jetové produkce / Investigation of the theoretical uncertainties in the jet production kinematics

Pokyny pro vypracování:
Různé modely výpočtů QCD produkce jetů předpovídají lehce odlišné chování jetů v koncovém stavu, především jejich počet, energii a prostorové uspořádání. Prozkoumejte dostupné modely, stanovte metodu porovnávání a analyzujte rozdíly v jejich předpovědích. Sledované modely by se měli lišit především v metodě výpočtu maticového elementu, v partonových distribučníchfunkcích, v silné vazbové konstantě α_S. Příkladem metody může být porovnání úhlového rozdělení jetů. Cílem studie bude následné porovnání s měřením v datech z experimentu ATLAS.

Součástí zadání výzkumného úkolu je jeho uložení na webové stránky katedry fyziky.

Literatura:

1. Kepka O., QCD analýza multijetových případů v proton-antiprotonových srážkách na urychlovači Tevatron, Diplomová práce MFF UK, 2006
2. Abazov V. M. et al. (D0 Collaboration), Measurement of Dijet Azimuthal Decorrelations at Central Rapidities in ppbar Collisions at sqrt(s)=1.96 TeV, Phys. Rev. Lett. 94, 221801, 2005
3. Khachatryan V. et al. (CMS Collaboration), Measurement of dijet azimuthal decorrelation in pp collisions at $\sqrt{s}$= 8 TeV, Eur. Phys. J. C76 (2016) 536
4. Malaescu B., Starovoitov P., Evaluation of the Strong Coupling Constant alpha_s Using the ATLAS Inclusive Jet Cross-Section Data, Eur. Phys. J. C72 (2012) 2041

Datum zadání: 27.10.2017 .....

Datum odevzdání: 30.06.2018 ***vedoucí katedry***

Prohlášení:

Prohlašuji, že jsem tuto práci vypracoval samostatně a použil jsem pouze podklady uvedené v přiloženém seznamu.

Nemám závažný důvod proti použití tohoto školního díla ve smyslu § 60 Zákona č. 121/2000 Sb., o právu autorském, o právech souvisejících s právem autorským a o změně některých zákonů (autorský zákon).

Prague, September 24, 2018 Vladimír Žitka

Název práce:

Výzkum vlivu teoretických neurčitostí na kinematiku jetové produkce

Autor: Vladimír Žitka

Obor: Experimentální jaderná a částicová fyzika

Druh práce: Výzkumný úkol

Vedoucí práce: Ing. Miroslav Myška Ph.D., FJFI ČVUT v Praze

Abstrakt: Cílem tohoto výzkumného úkolu je posktnout náhled do problematiky teoretických neurčitostí kinematiky jetové produkce. Jako zdroje této neučitosti jsou brány komplexní modely simulací protonových srážek. Speciální pozornost je pak věnována neurčitosti při volbě vazbové konstanty silné interakce, α_S Vzhledem k tomu, že její hodnota není přímo měřitelná, je důležité pochopit principy použité při jejím určování. Z tohoto důvodu je jedna kapitola věnována popisu různých způsobů nepřímého měření silné vazbové konstanty a jejich výhodám a zádrhelům. Stěžejní část této práce se věnuje rozboru analýzy čtyř různých sad dat získaných pomocí různých Monte Carlo modelů. Tyto modely byly: LO QCD Pythia, LO QCD Herwig, LO Matchbox a NLO Matchbox. V rámci této analýzy je porovnán vliv variací α_S v rámci modelů LO Pythia a LO Matchbox Herwig na tvar normalizovaých spekter příčné hybnosti, pseudorapidity a azimutální úhlové dekorelace, s vlivem změny modelu jako takového.

Klíčová slova: Pythia, Herwig, Silná vazbová konstanta

Title:

Investigation of the theoretical uncertainties in the jet production kinematics

Author: Vladimír Žitka

Specialisation: Experimental nuclear and particle physics

Type of thesis: Research project

Supervisor: Ing. Miroslav Myška Ph.D., FNSPE CTU in Prague

Abstract: The goal of this Research project is to provide an insight into theoretical uncertainties in jet production kinematics. Sources of these uncertainties are complex models of simulating proton collisions. Special attention is given to the uncertainties stemming from the choice of coupling constant of the strong interaction α_S. As the value of α_S cannot be measured directly it is important to understand the methods of its testing. To this end, a chapter has been dedicated to the techniques of indirect measurement of α_S and their advantages and downsides. This thesis culminates in an analysis of data sets acquired from four different Monte carlo models: LO QCD Pythia, LO QCD Herwig, LO Matchbox and NLO Matchbox. The influence of α_S variation on shape of normalised spectra of transverse momentum, pseudorapidity and azimuthal angular decorelation within LO Pythia and LO Matchbox models is compared with the influence of the generators them selves.

Key words: Pythia, Herwig, Strong coupling constant

Contents

List of Figures

Chapter 1

Standard model of particle physics

As the main objective of this thesis is the study of theoretical uncertainties of the theory of strong interactions on kinematic variables of particle jet production. It is only natural to present a brief overview of the standard model(SM) of particle physics, of which the strong interaction is an important part. Throughout this thesis, the reader is expected to be familiar with such concepts as particle jet, jet algorithms and basic kinematic variables used for describing them such as transverse momentum or pseudorapidity. In this thesis, the standard natural units notation is used: $c = \hbar = 1$.

1.1 Elementary particles

Every elementary particle is a manifestation of its quantum field and can be viewed as its material fluctuation. Every particle can exist only within the boundaries of Heisenberg uncertainty principle. This means that even if the energy available in system is not sufficient to reach the mass of the particle, the particle can be said to exist withing a sufficiently small time window. Each particle is characterized by its mass, lifetime and a set of various quantum numbers for example intrinsic angular momentum (spin), electric charge and colour charge (charge of the strong interaction), parity, flavour and lepton number. The common classification is into quarks, leptons and intermediate bosons. A brief overview of their properties can be found in Fig. 1.1. It should be mentioned, that bosons are generally particles with integral spin and so the particles in Fig. 1.1 are not the only bosons in existence. Quarks and leptons are included in the category called fermions, those are particles with half-integral spin that abide the Pauli exclusion principle.

Quarks: As can be seen in Fig. 1.1 there are three generations of quarks with each generation more massive than the other. In each generation there are

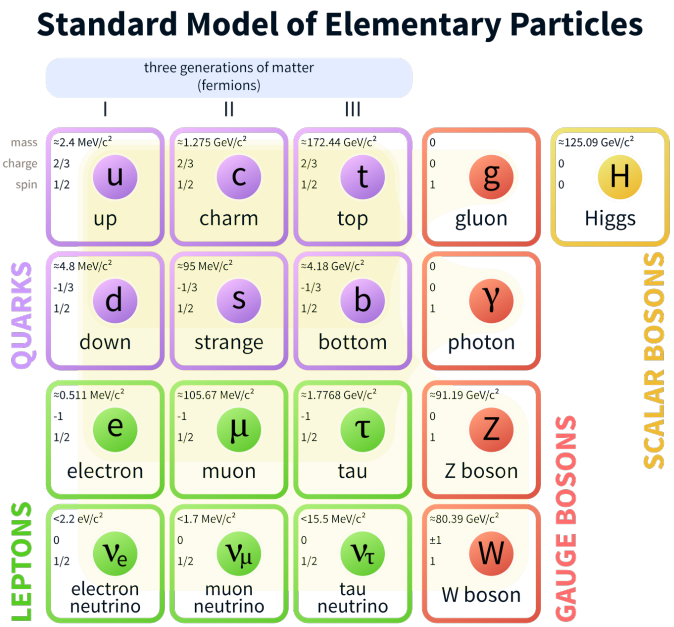

Fig. 1.1: A table of quarks, leptons and intermediate bosons. [23]

two quarks with different mass and charge. Each quark has its flavour, three colours and the charge of either $-\frac{1}{3}$ or $+\frac{2}{3}$ of elementary charge (e). This means that quarks are susceptible to all four interactions. Another interesting property of quarks is that they can never be found isolated and are ever in a bound into composite particles called hadrons. This property is more thoroughly discussed in the following chapter, along with other properties of quantum chromodynamics. Hadrons can be divided into mesons (bound states of a quark and an anti-quark, another example of bosons) and baryons (fermions that have three valence quarks).

Leptons: Those are the particles that do not participate in the strong interaction. They have the electric charge of either -1 e for electron, muon and tauon or 0 for their neutrinos.

Intermediate Bosons: The last category of particles shown in Fig. 1.1 is intermediate bosons. The gauge bosons, are the quanta of strong (8 gluons), weak (W^+,W^- and Z^0) and electromagnetic (photon) field. The one scalar boson is the Higgs boson which is the boson that belongs to higgs field - the field that causes through interaction with all the other fields that their quanta gain their mass.

1.2 Fundamental interactions

The four forces above are all except for the gravitational described in terms of quantum field theory. And the theory that describes the behaviour of Electromagnetic, Weak and Strong interaction together is called the Standard Model (SM) of particle physics. The gravitational interaction is the weakest interaction and plays almost no role in particle physic (except for experiments like AeGiS or GBar that explore the effects of gravity on antimatter). Gravity is described using general relativity that is separate from SM and is omitted in this thesis.

1.2.1 Weak interaction

It is the weakest of the three interactions in SM with about $1.166 \cdot 10^{-5}$ the strength of the strong interaction at the m_Z scale [19]. Its quantum field formulation is called Quantum Flavour Dynamics (QFD), although this name is rarely used. It can affect every known particle but it has a finite range of about 10^{-18} m because of the high mass of its gauge bosons. The high mass is a consequence of spontaneous symmetry breaking caused by the Higgs mechanism. It is interesting that existence of the boson Z was discovered and explained first after unification of the electromagnetic and weak interaction into one Electoweak (EW) theory and the subsequent discovery of neutral currents in data measurement. Up until that point it was thought that there were only the charged bosons $W^{\pm}$ that are responsible for the β-decay of nuclei.

1.2.2 Electromagnetic interaction

It has the middle strength in the SM with about $\frac{1}{137.035}$ the strength of the strong interaction [19]. Its quantum field formulation is called Quantum Electrodynamics (QED). It can only influence particles that carry electric charge and it has infinite range due to the zero mass of photon. It is the best known interaction and is described by the Maxwell equations. It is the interaction that governs our day-to-day life because it binds electrons and nuclei into atoms and atoms into molecules and even light itself is an electromagnetic field.

1.2.3 Strong interaction

It is the strongest known interaction. Its quantum field formulation is called Quantum Chromodynamics (QCD). It influences only particles that carry colour charge(there are three colours and three anti-colours)but it has a finite range of about 10^{-15} m which is roughly the diameter of a proton. This of course does not mean that the interaction does not reach beyond this threshold and the remnant force that remains is the nuclear force that binds nuclei together in a loose analogy to the Van der Waals force, a remnant of EM interaction, that can bind atoms into molecules. A more thorough description of QCD is in the following chapter about the proton scattering and the properties of QCD

1.2.4 Standard model

The Standard Model of particle physics is the theory that binds together the three interactions above along with the Higgs mechanism into one compact theory. The Lagrangian of this theory is rather extensive and so it is not mentioned here because it plays only a background role in the context of this thesis as an underlying principle. The main theoretical idea behind its construction was that it should be invariant under the groups of symmetries SU(3)×SU(2)×SU(1) from which properties and/or existence of elementary particles arise. It describes how quarks and leptons come to be and how they acquire their mass through the Higgs mechanism. Another part is describing the electroweak interaction and the breaking of the SU(2) symmetry that causes gauge bosons of weak interaction to gain mass. Yet another part describes the existence of colour and why there are 8 gluons (this is caused by the fact that the Lagrangian is invariant under the group of SU(3)). The last part of the Lagrangian deals with the virtual particles. It is clear that the standard model is not perfect as evidenced by observations of neutrino oscillations that hint at the non-zero mass of neutrinos which is in contradiction with the SM condition that the neutrinos have similar to the photon zero mass. However this does not mean that SM is completely wrong because its predictions are in many experiments highly precise.

Chapter 2

Proton scattering and QCD

The aim of this project is to shed light on the influence of certain theoretical uncertainties on the kinematics of jet production. The chosen property that is studied is the strong coupling. Its influence is studied in proton-proton collisions at LHC at the centre of mass energy of 13 TeV. It is useful to recapitulate the basic principles of scattering processes. The fundamental theory that describes the dominant proton scatterings at the LHC is Quantum Chromodynamics (QCD). However it is impossible at the moment to describe proton proton scattering using only basic QCD principles, the crux being the composite structure of a proton.

2.1 Proton structure

The first hints at proton being a composite particle came from electron-proton scatterings at SLAC and DESY at beam energy between 1 and 20 GeV. Similar structure in electron-proton has been observed in the secondary electron spectres as in electron-nucleus scattering which was a clear sign of inner structure. Later these components of proton have been identified as quarks. The cross section of elastic scattering of electron on proton that takes into account spin as well as magnetic moment of proton, in dependence on the square of four-momentum transfer $Q^2 = -\mathbf{q}^2 = (\mathbf{k} - \mathbf{k}')^2$, has been derived by Rosenbluth and can be written as:

$$\left(\frac{d\sigma}{d\Theta}\right)_{Rsb} = \frac{2\alpha^2 E^2}{Q^4} \frac{\cos^2(\theta/2)}{1 + \frac{2E}{m_p}\sin^2(\theta/2)} \left[A(Q^2) + B(Q^2)\tan^2\frac{\theta}{2}\right], \qquad (2.1)$$

where $A(Q^2)$ and $B(Q^2)$ are formfactors:

$$A(Q^2) = \frac{G_E(Q^2) + \left(\frac{Q^2}{4m_p^2}\right) G_M(Q^2)}{1 + \frac{Q^2}{4m_p^2}},$$
$$B(Q^2) = \frac{Q^2 G_M(Q^2)}{2m_p^2}$$

The dependence of both formfactors is in good agreement with an experimentally determined dipole formula:

$$G(Q^2) = \frac{1}{\left(1 + \frac{Q^2}{m^2}\right)^2} \tag{2.2}$$

The relation between both proton formfactors is quite simple: $G_E^p = \frac{G_m^p}{\mu_m^p}$ where μ_m^p is the anomalous magnetic moment of proton.

As values of Q^2 increase the overall importance of elastic scattering decreases and inelastic scattering rises into prominence. Let us consider the process $ep \to eX$ where X is a hadron system with the invariant mass W. The square of invariant mass in laboratory frame is $W^2 = (\mathbf{p} + \mathbf{q})^2 = 2m_p\nu + m_p^2 + q^2$, where ν is the transfered energy and $\mathbf{p}$ is the four momentum of proton in laboratory frame with the component $(m_p, 0, 0, 0)$. Therefore

$$Q^2 = 2m_p\nu = m_p^2 - W^2. \tag{2.3}$$

In case of inelastic scattering W^2 can differ from m_p^2 which means that Q^2 and ν are independent variables. The differential cross section of inelastic $e - p$ scattering in laboratory frame can be written in similar form as (2.1):

$$\frac{d^2\sigma}{d\Omega dE'} = \frac{4\pi\alpha^2 E'^2}{Q^4}\left[W_2(Q^2,\nu)\cos^2\frac{\theta}{2} + 2W_1(Q^2,\nu)\sin^2\frac{\theta}{2}\right], \tag{2.4}$$

where $W_1(Q^2,\nu)$ and $W_2(Q^2,\nu)$ are so called structure functions of proton which replace the elastic fromfactors G_E and G_M. Inelastic processes are best described by the momentum transfer Q^2 and the Bjorken variable $x = \frac{Q^2}{2\mathbf{pq}}$. For elastic scattering is $x = 1$ and for inelastic is always $x < 1$ because $W^2 > m_p^2$. For low x and high Q^2 there is the region of the Deep Inelastic Scattering (DIS). Meaning of DIS is that the inner structure of proton comes into play. In 1969, Richard Feynman has proposed a hypothesis that DIS cross section of electron on proton can be expressed as a composite spectrum of elastic scatterings of electron on partons, that carry only a portion of the whole momentum of the whole proton, this portion being expressed by the Bjorken x. [13] Assuming that partons are spin 1/2 particles, we can express the cross section for scattering of electron on i-th parton as:

$$\frac{d^2\sigma^i}{d\Omega dE'} = \frac{4\pi\alpha^2 E'^2}{Q^4}\left[e_i^2\cos^2\frac{\theta}{2} + e_i^2\frac{Q^2}{2m_i^2}\sin^2\frac{\theta}{2}\right]\delta(\nu - \frac{Q^2}{2m_i}), \tag{2.5}$$

where e_i is the charge of parton expressed in units of positron charge. As every parton carries different part of the momentum x, it is necessary to multiply the cross section (2.5) by a weighting function $f_i(x)$ that defines the probability that parton i carries fraction of momentum x before adding it into the composite DIS cross section. Approximating that the electron-parton scattering leaves the state of other partons unchanged, the whole cross section of electron proton can be expressed as following sum:

$$\frac{d^2\sigma}{d\Omega dE'} = \sum_i \int_0^1 \frac{d^2\sigma^i}{d\Omega dE'} f_i(x)dx. \tag{2.6}$$

A new form of expression of the structure functions W_1 and W_2 can be obtained by comparing (2.4) and (2.6):

$$m_p W_1(\nu, Q^2) \equiv F_1(x) = \sum_i \frac{e_i^2}{2} f_i(x) \tag{2.7}$$

$$\nu W_2(\nu, Q^2) \equiv F_2(x) = \sum_i e_i^2 x f_i(x). \tag{2.8}$$

It is rather obvious that the new structure functions F_1 and F_2 depend exclusively on x, this property is known as Bjorken scaling. Their relationship is summarised into the Callan-Gross relation:

$$2xF_1(x) = F_2(x) \tag{2.9}$$

that holds only if the spin of parton is 1/2, which has been experimentally confirmed in the SLAC laboratory. [14] This exclusive dependence on Bjorken x holds for $x \gtrsim 0.05$ as is demonstrated in Fig. 2.1. This is discussed below after the introduction of running coupling.

This experimental proof has been one of the reasons that partons have been identified as quarks. Those have been successfully used for explaining some static hadron properties. Quantum numbers of a proton can be explained using the assumption that the proton consists of two up(u) a one down(d) quarks. Those are called valence quarks. The same numbers can be obtained if proton contains any number of additional quark-antiquark pairs, because their additive quantum numbers are equal to zero. Those are called the see quarks. Let $f_i(x)$ denote the parton distribution function(PDF) of the parton i in a nucleon. It is possible to express any PDF in the form of a distribution function for valence and see quarks:

$$f_i(x) = V_i(x) + S_i(x). \tag{2.10}$$

If the only flavours that are taken into account are up, down and strange, the structure functions of proton and neutron can rewritten as:

$$F_2^{ep} = \frac{x}{9}[4V_u(x) + V_d(x)] + \frac{4}{3}xS(x),$$
$$F_2^{en} = \frac{x}{9}[V_u(x) + 4V_d(x)] + \frac{4}{3}xS(x),$$

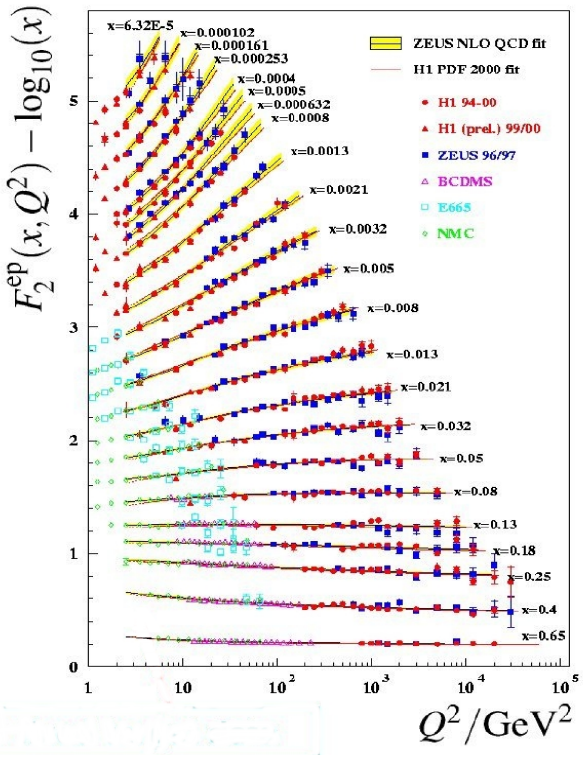

Fig. 2.1: The dependence of structure function $F_2(x, Q^2)$ on the momentum transfer Q^2.

where V_i are the valence quark PDFs and S is the sea quarks PDF (assuming that all see quarks have the same distribution). The V_s and those of antiquarks have been omitted due to them being equal to zero as expected.

Considering scattering of a proton on a nucleus with equal number of protons and neutrons, a average structure function of a nucleon N can be expressed as:

$$F_2^{eN} = \frac{1}{2}(F_2^{ep} + F_2^{en}),$$

$$F_2^{eN} = x\left[\frac{5}{18}[f_u(x) + \overline{f}_u(x) + f_d(x) + \overline{f}_d(x)] + \frac{1}{9}[f_s(x) + \overline{f}_s(x)]\right]$$

It would be reasonable to expect, that the summed momentum of partons should be equal to the momentum of the proton, i.e.:

$$\int_0^1 x[f_u(x) + \overline{f}_u(x) + f_d(x) + \overline{f}_d(x) + f_s(x) + \overline{f}_s(x)]dx = 1$$

Therefore it could be assumed that, approximating the influence of strange quarks as negligible:

$$\frac{18}{5}\int_0^1 F_2^{eN} dx \simeq 1.$$

However the experimental value derived from cross sections of charged leptons on nucleus of carbon is around 0.5, which means that quarks and antiquarks share only about half of the whole momentum of a nucleon. The rest of the momentum is carried away by other components that are inside a nucleon but are invisible to the electromagnetic and weak force. These components are called gluons and have no electric or weak charge, but they do have colour charge. The direct consequence of gluons carrying colour charge is that they are capable of interacting with themselves, this property and its other consequences are discussed in the followign section. The distribution of momentum carried by gluons is characterised by the gluon distribution function, usually denoted $g(x)$.

2.2 Quantum Chromodynamics

Now it is time to introduce QCD in greater detail. QCD is a non-abelian gauge theory which is based on the $SU(3)$ colour gauge group due to the fact that QCD has to comply to several experimental and theoretical conditions such as the existence of $q\bar{q}$(mesons),qqq(baryons) and potential tetra- or penta-quark bound states, asymptotic freedom of quarks and long range cut-off of the strong interaction. From the existence of bound states such as Δ^{++} which has three identical quarks, the need for three different colour states(red, green and blue) can be derived. To this day, the existence of tetra- and penta-quarks is the subject of intense studies for example at the LHCb experiment such as [3] for tetra-quarks and [4] for penta-quarks. Expecting the particle/antiparticle symmetry one arrives to:

$$3 \otimes 3 = 1 \oplus 8 \tag{2.11}$$

which gives the colour octet of gauge bosons = gluons that supply the colour interaction and one colour singlet that does not. The colour octet states of gluons are:

$$\frac{1}{\sqrt{2}}(r\bar{b} + b\bar{r}) \qquad \frac{-i}{\sqrt{2}}(r\bar{b} - b\bar{r})$$

$$\frac{1}{\sqrt{2}}(r\bar{g} + g\bar{r}) \qquad \frac{-i}{\sqrt{2}}(r\bar{g} - g\bar{r})$$

$$\frac{1}{\sqrt{2}}(b\bar{g} + g\bar{b}) \qquad \frac{-i}{\sqrt{2}}(b\bar{g} - g\bar{b})$$

$$\frac{1}{\sqrt{2}}(r\bar{r} - b\bar{b}) \quad \frac{-i}{\sqrt{6}}(r\bar{r} + b\bar{b} - 2\,g\bar{g})$$

and the colour singlet state is:

$$\frac{1}{\sqrt{3}}(r\bar{r} + b\bar{b} + g\bar{g}).$$

The lagrangian of quantum chromodynamics has a standard form [20]:

$$\mathscr{L}_{QCD} = \overline{\psi}(i\gamma^\mu \mathscr{D}_\mu - m)\psi - \frac{1}{2}\mathrm{Tr}(G_{\mu\nu}G^{\mu\nu}), \tag{2.12}$$

where ψ is the spinor colour triplet of quarks

$$\psi = \begin{pmatrix} q_r \\ q_b \\ q_g \end{pmatrix}, \tag{2.13}$$

and $\mathscr{D}_\mu$ is the covariant derivative :

$$\mathscr{D}_\mu = \partial_\mu + igB_\mu \tag{2.14}$$

where B_μ is a 3x3 matrix in colour space composed from colour gauge fields b^l_μ and the generators of the $SU(3)$ group $\lambda^l/2$:

$$B_\mu = \frac{1}{2}\lambda \cdot \mathbf{b}_\mu = \frac{1}{2}\lambda^l b^l_\mu. \tag{2.15}$$

The $G_{\mu\nu}$ in (2.12) is the gluon field-strength tensor:

$$G_{\mu\nu} = (ig)^{-1}\left[\mathscr{D}_\nu, \mathscr{D}_\mu\right] = \partial_\nu B_\mu - \partial_\mu B_\nu + ig[B_\nu, B_\mu].$$

A more in-depth discussion of properties of the λ matrices, along with more rigorous derivation of QCD as group theory can be found for example in [20]. Following paragraphs are focused more on a few crucial aspects and properties of QCD and its' perturbative variant.

2.2.1 Running coupling

One of the key things about QCD is the value of its coupling constant which can serve as an expression of the relative strength of QCD in comparison with the other interactions. The definition of coupling constant of the strong interaction is standard:

$$\alpha_S = \frac{g^2}{4\pi}, \tag{2.16}$$

where g is the dimensionless coupling constant from the definiton of covariant derivation (2.14) and gluon strength tensor $G_{\mu\nu}$.

The value of α_S is important mainly in perturbative QCD (pQCD) where observables are usually expressed in terms of the renormalized coupling. Contrary to what its name suggests, α_S is not constant, but has dependency on the (non-physical) renormalization scale μ^2_R. In order to compare the strength of QCD, the value of renormalization scale must be close to the value of momentum transfer: $\alpha_S(\mu^2_R \simeq Q^2)$. The behaviour of the value of α_S in relation to Q^2 is called the running coupling and is governed by the renormalization group equation [19]:

$$\mu_R^2 \frac{d\alpha_S}{d\mu_R^2} = \beta(\alpha_S) = -(c_0\alpha_S^2 + c_1\alpha_S^3 + \ldots), \tag{2.17}$$

$$c_0 = \frac{33 - 2n_f}{12\pi} \tag{2.18}$$

$$c_1 = \frac{153 - 12n_f}{24\pi^2} \tag{2.19}$$

where the c_k are the $(k+1)$-loop β-function coefficients, n_f is the number of quark flavours considered light ($m_q \ll \mu_R$). The precise value of loop coefficients c_k depends on the renormalization scheme with the value given here coming from the most widely used modified minimal subtraction scheme ($\overline{MS}$). If all, but c_0 loop coefficients are neglected and the number of flavours is taken asi constant, then the exact analytic solution for equation (2.17) is

$$\alpha_S(\mu_R^2) \;=\; \frac{1}{c_0 \ln\left(\frac{\mu_R^2}{\Lambda^2}\right)}. \tag{2.20}$$

The Λ is a constant of integration which denotes the scale where the perturbative coupling would diverge. Its value indicates the energy range where non-perturbative effects dominate. Because the exact value of Λ that defines the value of α_S is scheme and n_f dependent, the standard practice for quoting the value of α_S is to state the value at a given scale, typically mass of Z boson M_Z instead of at the value of Λ.

An example of the running coupling can be seen in the Fig. 2.2 along with the comparison of shift of the curve that is caused by using a different renormalization scheme.

More detailed discussion of the effects of different renormalization schemes and n_f values on the running coupling can be found in [12].

As was demonstrated in Fig. 2.1, the constant behaviour of structure function breaks down for small values of Bjorken x. This behaviour can be explained using renormalization procedures which yield the Dokshitzer-Gribov-Lipatov-Altarelli-Parisi(DGLAP) parton evolution equations (2.21) and (2.22) for redefining the quark an gluon PDFs into their renormalized forms where the factorization scale μ_F is introduced to ensure the logarithmic scaling.

$$\frac{\partial f_i(x,\mu_F^2)}{\partial \log \mu_F^2} = \frac{\alpha_S}{2\pi}\int_x^1 \frac{dz}{z}\left[P_{q_iq_j}(z,\alpha_S) f_j(\frac{x}{z},\mu_F^2) + P_{q_ig}(z,\alpha_S) g(\frac{x}{z},\mu_F^2)\right], \tag{2.21}$$

$$\frac{\partial g(x,\mu_F^2)}{\partial \log \mu_F^2} = \frac{\alpha_S}{2\pi}\int_x^1 \frac{dz}{z}\left[P_{gq_j}(z,\alpha_S) q_j(\frac{x}{z},\mu_F^2) + P_{gg}(z,\alpha_S) g(\frac{x}{z},\mu_F^2)\right], \tag{2.22}$$

The $P_{ab}(z,\alpha_S)$ are splitting functions, where first index denotes the final state particle that carries the momentum fraction z and the second index is the initial particle that undergoes splitting. Usually the factorization scale μ_F is taken to be identical to the renormalisation scale μ_R

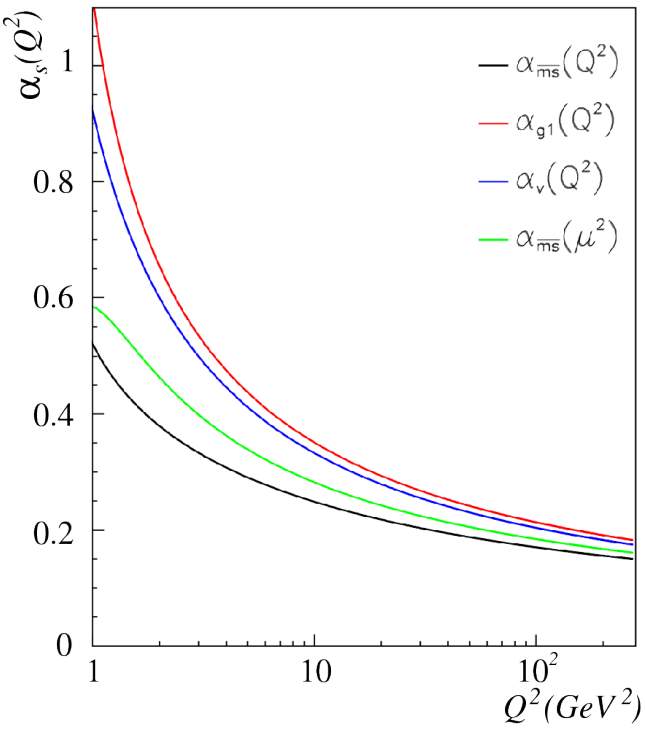

Fig. 2.2: The demonstration of the effect of different renormalization schemes on the running coupling of QCD. [12]

2.2.2 Colour confinement and asymptotic freedom

One of the interesting properties of quantum chromodynamics is the phenomenon of asymptotic freedom. That is if a colour charge is inspected under small space scales, in other words in processes with high momentum transfer, the value of strong coupling is falling precipitously as can be seen in Fig. (2.2). As a result of this low value of α_S, the relative strength of force that is affecting a colour charge is falling and the charge can behave almost freely. Other interpretation can be that the effective colour charge of the object is distorted by creation of pairs of colourful objects such as quark and gluon loops as is demonstrated in Fig.2.3.

On the other hand, α_S rises as a logarithm at larger distances/smaller momentum transfers. However due to the fact, that proton has a finite size this growth cannot be indefinite. This means that the colour charge has to be confined. That in turn implies existence of a certain cutoff for the value of α_S. The specific value of this cutoff is the subject of phenomenological studies and is omitted.

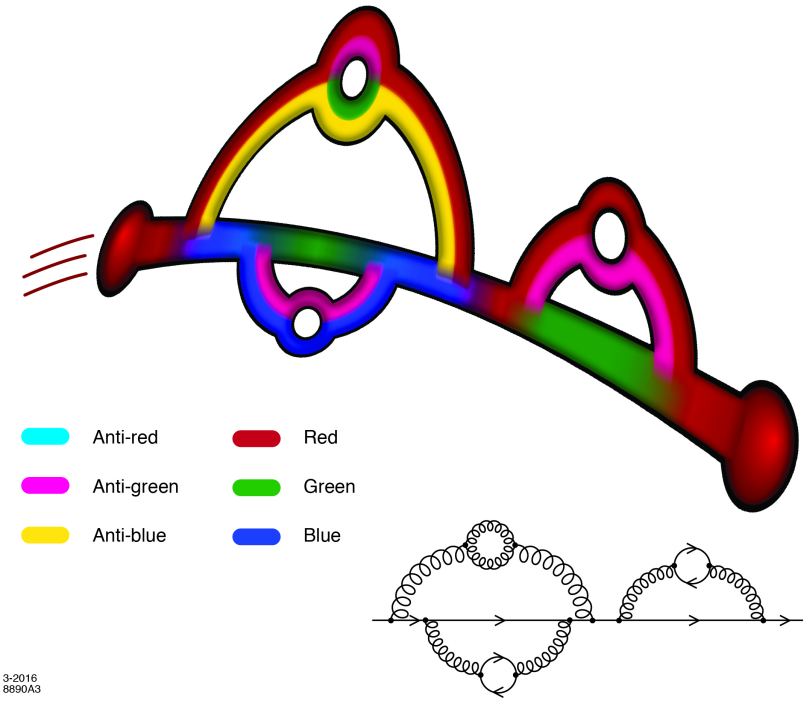

Fig. 2.3: Demonstration of colour charge antiscreening via the creation of quark and gluon loops. [12]

Chapter 3

Review of methods for measurement of α_S

The aim of this chapter is to put forth a brief overview of the methods of measurement of α_S that are, or have been, used. The value of strong coupling can be evaluated using a number of different measurement techniques that involve hadronic processes. Some constraints can be obtained from lattice gauge theory calculation, however those exceed the frame of this thesis. The comparison between the various methods of measurement can be drawn by evolving them to a common scale, typically the mass of the Z boson M_Z. The evolution of the world average value of the strong coupling constant as compiled by the Particle Data Group in 2014 can be found in Fig. 3.1.

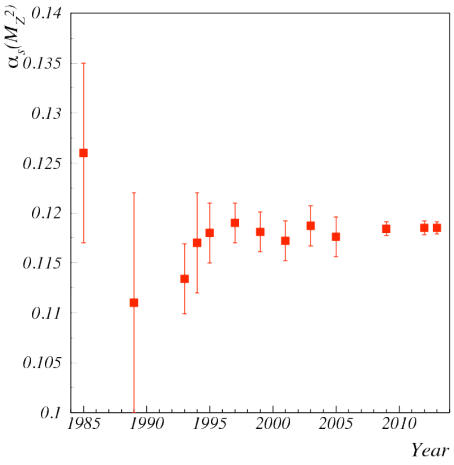

Fig. 3.1: The evolution of the value of strong coupling constant since 1990. [18]

There is a clear shift towards high precision measurements in the last years.

The present range of momentum transfers that has been used for measurement is $(0.05 < Q^2 < 10^3)\text{GeV}^2$, although in order to safely evolve the data with well controlled perturbative equations, the Q^2 should be at least above one GeV^2. A compilation of results from a few different methods of measurement can be found in Fig. 3.2

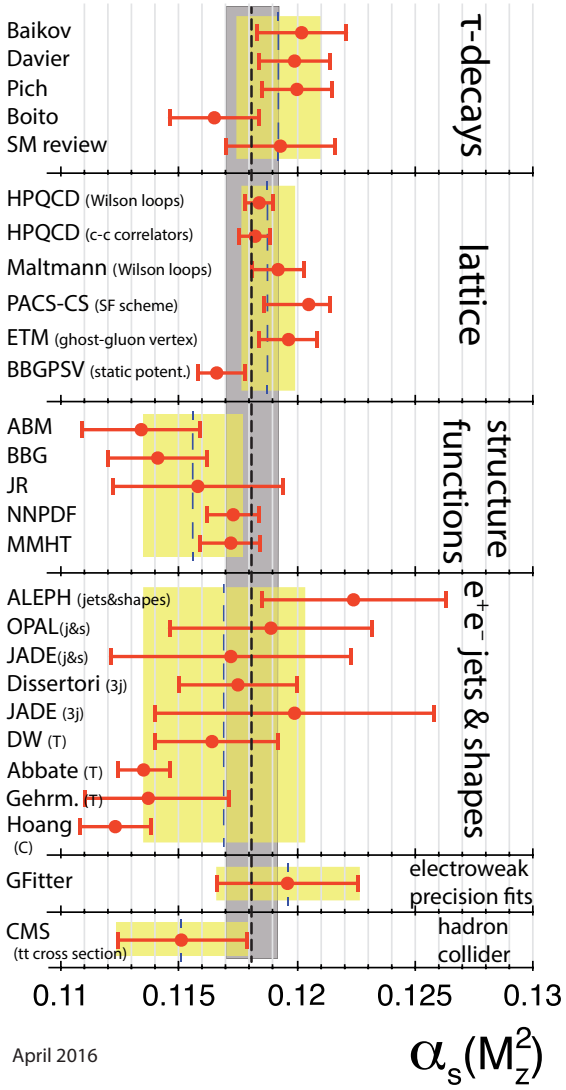

Fig. 3.2: An overview of the values of α_S as compiled by the Particle Data Group in 2016. [19]

Due to the overall agreement between the methods of determination, the

conclusion can be drawn that the pQCD is rather consistent throughout the Q^2 range. Nevertheless there are still inconsistencies between various measurements, those are however attributed more to the underestimation of uncertainties, rather than failure of QCD or effects from physics beyond the Standard Model. The descriptions of a few measuring methods are the content of following sections. A more detailed discussion and description of measuring methods and their pros and cons can be found for example in [12, 21]

3.1 Deep Inelastic Scattering

The concept of DIS has been introduced in previous chapter. The main sensitivity of the inclusive DIS data stems from violation of Bjorken scaling induced at LO by gluon bremsstrahlung from the struck quark as well as photon-gluon fusion and pair creation processes that are underlying the pQCD. DIS data provide the most robust way to obtain α_S, the argument being that the observables (the nucleon structure function $F_2(x, Q^2)$ and the gluon distribution $g_1(x, Q^2)$) are fully inclusive and therefore have no uncertainties from final-state hadronic corrections.

The precision of α_S from DIS is in order of percents due to the high precision of the measurements of the structure function $F_2(x, Q^2)$ over a wide kinematic range. The biggest uncertainty in this case comes from the uncertainties of the gluon density distribution where theoretical understanding of the underlying evolution is well developed, but the precision of data is a bit lacking.

Another possible observable for determination of α_S come from jet production in DIS. For example the production rate based on the subprocess $\gamma^* q \rightarrow qg$ is directly proportional to α_S. The processes underlying the production of gluon jet are the same ones as with the Q^2 dependence of DIS structure functions. The correct kinematic domain is high Q^2 and large mean transverse energy of the two leading jets. The value of α_S can be then extracted from the resulting scaling violations. The precision is then limited by the correlation between α_S and the gluon distribution. The advantage of this approach is the ability to directly measure the Q^2 dependence of the strong coupling.

3.2 Collision of e^+e^-

Observables from the e^+e^- provide more inclusive processes used for extraction of α_S. In leading order approximation, the electron annihilates with positron radiating a virtual photon or a Z boson which in turn decays into quark and antiquark pair.

In the vicinity o the Z-boson pole the thinkable observables are:

- decay width Γ_Z
- ratio $R_Z = \frac{\Gamma_Z(hadrons)}{\Gamma_Z(leptons)}$
- hadronic and leptonic cross sections.

The leptonic cross section incorporates the Γ_Z and therefore is sensitive to α_S. In the domain away from the pole the production of virtual photons is competing with the Z production. The ratio of hadron production to lepton production can be measured and in each case the sensitivity to α_S comes from the decay width Γ_Z and its predominant hadronic decays. The two cases have another advantage in that their experimental setups are different and easily distinguishable which yields independent and uncorrelated experimental systematic uncertainties. The main influence of α_S on these measurements stems at LO from bremsstrahlung on the $q\overline{q}$ lines into which the Z boson or photon have decayed. Similarly to DIS, the corrections from vertex and self-energy enter at NLO.

One of the important final states in the lepton channel of Z decay is the $\tau\overline{\tau}$ one. It is especially useful for the extraction of α_S at low momentum scale $M_\tau = 3.157$ GeV [9]. The method of extraction is again based on the ratio of hadronic to leptonic decay, this time for the τ meson. The downside of this method is that the higher pQCD corrections as well as nonperturbative effects step into fray at these low Q^2 scales.

Another measurement of α_S comes from the analysis of Q^2 dependence of the average gluon and quark jet multiplicities using an improved formalism shown in [8]

3.3 Proton-proton collisions

One of the methods of extraction of α_S from proton collisions is through fitting the measured values of p_T spectra and other observables using different PDF sets, all with variations in α_S as well, and then using statistical tools to determine the average value and its precision. These studies typically demand the use of NLO QCD predictions in order to achieve competitive precision. An example of such an analysis has been done by the ATLAS collaboration in 2012 [17]. There are four different PDF sets used for simulation of inclusive jet cross sections in several p_T and rapidity bins. Within every PDF set, the value of α_S is varied with the step of $d\alpha_S = 0.0001$ from the appropriate extreme values, provided by the respective author of each PDFset. The simulations are then analysed using two different jet radii. Then the α_S is extracted using statistical methods such as simple and geometric average or χ^2/DOF minimalization. An example of α_S distribution extracted from simulations can be found in Fig. 3.3

The correlations between (pt, y) bins are then discussed as well in order to better understand the uncertainty of the resulting α_S value.

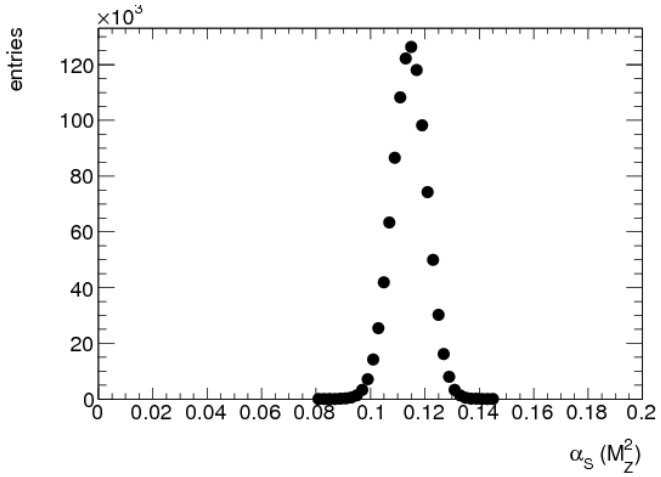

Fig. 3.3: An example of α_S distribution obtained from pseudo-experiments, for Anti-k_T jets with radius parameter $R = 0.6$ in the central rapidity region ($0 \leq |y| \leq 0.3$). [17]

Chapter 4

Analysis of theoretical uncertainties

This chapter is dedicated to the discussion of the influence the value of α_S has on the shape of a few selected variables in proton-proton collisions and if these effects have bigger influence than generator effects.

4.1 Motivation

One of the goals of this chapter and the thesis as a whole is to gain insight into the consequences of choosing a different values of the strong coupling constant during simulation of proton proton collisions. The exact value of the coupling can result in rather severe fluctuations in values of cross sections for processes such as the Higgs boson or top-quark production. The reduction of these cross sections is about $8-9\%$ going down from $\alpha_S = 0.118$ to $\alpha_S = 0.113$ according to [21]. This uncertainty is bigger than that from higher order corrections (about $4-6\%$ for Higgs [5]) or experimental uncertainties (about $3-4\%$ for $t\bar{t}$ production [2]). In order to justifiably neglect the α_S uncertainties, the value has to be known with precision higher than 1%. Because even at 1% this leads to uncertainties in cross sections that are comparable to any other single theoretical uncertainty [21].

Another goal is to asses the influence that the value of α_S has on the shape of the spectrum of the normalised dijet azimuthal angular separation:

$$\frac{1}{\sigma}\frac{d\sigma}{d\Delta\phi}. \tag{4.1}$$

This variable has been chosen in order to minimalize the influence of jet energy uncertainties as much as possible. That is beccause it is primarily space-related variable and the momentum of particles comes into play only indirectly during the clustering of particles using jet algorithm. The azimuthal angular separation has been also chosen because it has been measured several times by the CMS

collaboration at the LHC [11, 16] and thus can have a grounded comparison to data in future studies. However at this stage it is more important to analyse the influence of different generator types on the shape of these spectra.

4.2 Simulated data

The data used throughout this chapter are simulations of proton-proton collisions and have been generated using the Monte-Carlo generators Pythia 8.2.3.5 and Herwig 7.1.2. There has been generated six data sets for different values of α_S surrounding the central value that has been chosen as $\alpha_S(M_Z) = 0.118$, for both LO QCD Pythia and LO Matchbox Herwig models. The central value has been chosen as an approximation of the world average taken from [19] The values are:

$$\alpha_S \in (0.116, 0.117, 0.1175, 0.1185, 0.119, 0.120),$$

which is equivalent to variation of the α_S up to 1.7% from its default. Energy of collisions has in all cases been set to 13 TeV. In both cases, the data are processed using the Anti-k_T algorithm from FastJets library [10] in order to reduce the memory needed to store all particles. The output data have then the form of TTree structure where the branches contain the information about the event. Four branches of standard vectors of float type varibales that contain the p_T, η, ϕ and E of jets in current event. And two branches of simple float type variables containing the weight and cross section of current event.

The specifics of both generators are discussed in the following subsections.

4.2.1 Pythia

The main advantage of Pythia is in its simple applicability and malleability due to its structure as C++ library. The hadronization model implemented in Pythia is the Lund String Model, which is a phenomenological model based on the idea of stretching g-strings between colour charges and then combining them into colourless objects. The showering is separated into time-like and space-like showering and both are handled by a p_T ordered algorithm. More rigorous information on the hadronization and showering process can be found in the manual [22].

The data have been generated in Leading Order (LO) of pQCD, with the PDF NNPDF23-LO-as-0119-qed taken from the LHAPDF6 library along with the standard ATLAS tune A14 [1]. All data have been generated in 17 $\hat{p_T}$ bins with 10^6 events per bin in order to achieve sufficient amount of data throughout the whole kinematic range. The Pythia data set is used as a baseline to which the data sets generated using Herwig are compared. The integrated cross section of data generated by Pythia is $\sigma_{Pyt} = 0.115$ μb for jets with $p_T \in (100, 8000)$ GeV and $|\eta| < 4.8$

The downside of Pythia is the need to set the value of α_S for each process involved in generation of the data individually. This means that if one would wish so, the value could be different for the matrix element, Time-like

showering, Space-like showering and Multiparton interaction. Of course, such flexibility could be seen as an advantage if the aim were to study the influence of α_S on the individual processes, that is however not the case in this analysis. The flexibility has caused (in early stages of this analysis) a certain discord between the values of data generated using the value of α_S said to be default in the documentation and the data generated without the modification of values of α_S. The exact cause of this issue has not been identified, however one of the working theories were the use of an archaic PDF CTEQ and the lack of proper tuning, which have been amended in the current version of analysis.

4.2.2 Herwig

An advantage of Herwig is that there is only one central value of α_S that needs to be set. The hadronization model implemented in Herwig is the Cluster model, which is not as physically rigorous as the Lund String Model in Pythia. The cluster model simply combines the present colour charges into colourless objects and then treats these as decaying massive particles. The default showering algorithm used by Herwig is angular ordered. More information on Herwig can be found in the release note [6].

Another advantage is the ability to generate NLO precision data, through the Matchbox procedure, which allows to match an external matrix element(either LO or NLO) acquired from MadGraph-OpenLoops package with showering provided by Herwig. The main role of the matchbox procedure comes into play especially in NLO calculations. If the wish is to study the influence of α_S on the p_T spectra of jet production, it essentially comes down to generating processes of QCD 2 to 3 type, because the standard back to back jets fro QCD 2 to 2 are not really useful in this case. The 2 to 3 processes are by definition NLO. The matchbox is however very time-consuming. For this reason there is only one set of data, with $1.5 \cdot 10^6$ events, generated in NLO Matchbox, with the value of α_S left at default $\alpha_S(M_Z) = 0.118$ and the PDF MMHT2014. This NLO Matchbox dataset is included in order to have a approximation of the NLO behaviour. LO Matchbox generation has been done using the PDF MMHT2014 with default tune in six $p_{T,jet}$ bins with 10^6 events per bin and one inclusive sample with 10^7 events.

It is important to remark that there is a slight difference in the generation proceedings between Herwig Matchbox and Pythia. It concerns the generation in $\hat{p_T}$ ($p_{T,jet}$) bins. Where Pythia makes the cut on the p_T on the matrix element level, Herwig cuts are applied at the jet level, this means that there is ambiguity in the origin of the jets due to the matrix element having possible additional external lines(mainly in NLO). Because the $p_{T,jet}$ bins are not completely exclusive (the cut being applied only to the jet with the highest p_T) there is a need for a merging procedure that would produce a correct inclusive spectrum after the combination of data from all samples. Our working approach is to exclude all jets that does not fall into the appropriate bin. This produces a reasonably smooth p_T spectra, but at the cost of relatively high jet-rejection rates (circa 30%). Therefore it would be best to implement an additional merging algorithm

that would be more sophisticated and would have better rejection rate. For this reason, there is another data set generated by herwig with the pdf MMHT2014 in the leading order but with the matrix element QCD2to2 that is provided by Herwig by default with the integrated cross section of $\sigma_{QCD2to2} = 0.198$ μb. Here the rejection rate is much better due to the cuts taking place again at matrix element level, same as with Pythia.

The issue with Matchbox is that all generations are rather time consuming. Since version 7.1.0, Herwig has the option of using a reweighting procedure, which would greatly reduce the needed number of generated events, eliminate the need for generation in $\hat{p_T}$ bins and therefore shorten generation time [7]. The reweighting works with the premise of generating a flat spectrum of events and then shifting the weight of events according to their p_T and energy scale in order to achieve physical correctness. There has been an attempt to test this procedure in this analysis for the matchbox data, this has however proven to be difficult and has lead to issues such as negative cross sections and weights. For these reasons the reweighting has been left out of this analysis. Nevertheless the hope remains that should it be fixed in following versions of Herwig, the options for feasible NLO generations would open and the speed of LO generations would greatly increase.

4.3 Analysis of results

Now follows the presentation and discussion of the findings in this analysis. Throughout this section, the blue lines are representing the data sets generated by Herwig Matchbox LO, green lines for Herwig Matchbox NLO, red lines for default Herwig QCD 2 to 2 and black lines for Pythia LO, all of which are generated with the default values of $\alpha_S(M_Z) = 0.118$. The rest of the colours represents the variations in α_S as shown in Tab. 4.1.

$\alpha_S(M_Z)$	colour
0.116	crimson
0.117	orange
0.1175	yellow
0.1185	spring green
0.119	cyan
0.120	violet

Tab. 4.1: Colour coding of different α_S values.

4.3.1 Control variables

The control variables normalised transverse momentum p_T and normalised pseudorapidity η are to be found in Fig.4.1(a,b) and 4.3 respectively. The effects of generators are demonstrated in those figures without the additional α_S variations in order to keep the figures easy to take in. The effects of α_S variations on the shape of normalised p_T spectrum for Matchbox LO and Pythia Models can be found in Fig.4.2.

Over the course of this analysis, the influence of the value of α_S has proven to be less significant than that of the generator effects. This is demonstrated in Fig. 4.1(b,c,d) for the p_T spectra.

It is clear that the shape of the spectra is different for each generator in 4.1. The shape of p_T varies from Pythia LO up to 30% for the default Herwig QCD2to2 model, up to 40% for the Matchbox LO model and up to 70% for the Matchbox NLO model. However upon closer examination it has been discovered that the most violent shape variations occur at the border of each $\hat{p_T}$ used during the generation of respective data sets for each model. The best example is for the default QCD 2 to 2. What is interesting is that the variation in shape seems to be of opposite sign for the default QCD2to2 model and the Matchbox models. These deviations suggest an error in merging of the $\hat{p_T}$ samples that will have to be remedied before further analysis, for example by implementing the reweighting procedure mentioned in previous section, which would effectively eliminate the need for merging altogether. On top of this merging error, the NLO have large statistical errors in some regions. That shall be resolved by simply generating more data.

The consistency between generators is better in space - or so suggests the Fig.4.3. It seems that the Matchbox LO model produces more particles with higher pseudorapidities than Pythia. Nevertheless in the pseudorapidity region of the ATLAS inner detector $|\eta| < 2.5$, the shapes seem to be consistent within statistical fluctuations. This is true for the default QCD2to2 as well, although generally the situation for production rates for this model is reversed, and one can see a hint of a peak at zero and steeper drop outside the inner detector region. The worst consistency with Pythia has the Matchbox NLO that tends to produce more higher pseudorapidities. On the other hand these higher η regions have large statistical fluctuations and even the rest of the spectrum has bigger statistical uncertainties than the other models. This could play a role as well and with more data the shape could grow closer to the other generators.

The effects of different generators and merging of data samples throughout the p_T spectrum are roughly between 10% to 20%. The effect of α_S variations is especially for pythia in the range of units of per cent. The Matchbox model is not as consistent for the α_S variations, mainly in the region $p_T \in (200, 1000)$ GeV, but that is again probably caused by the merging of data samples than the actual effect of α_S variation, the reason for this suspicion is that no such fluctuations are present for Phythia data set that have been generated in much finer samples where the exponential drop within the sample would not be as severe.

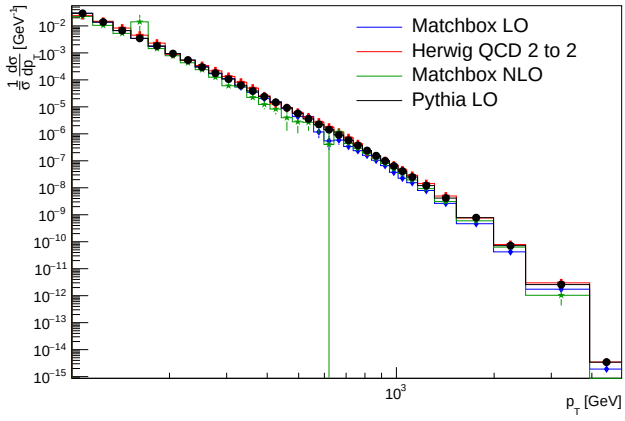

(a) Normalised spectrum

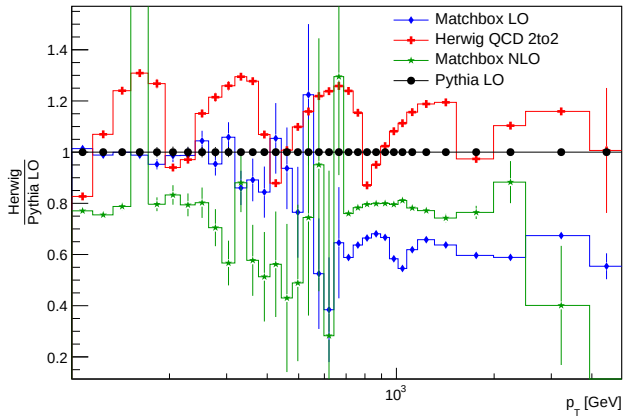

(b) Generator effects

Fig. 4.1: The normalised spectrum of transverse momentum for all four models and the ratio plots demonstrating the effect of α_S variation on the shape of the spectrum within Herwig Matchbox LO and Pythia LO models for jets with $|y| < 4.8$ and $p_T > 100$ GeV. Blue represents Herwig Matchbox in Leading Order. Red represents Herwig QCD2to2 in Leading order and green represents Herwig Matchbox NLO. Black represents Pythia LO

4.3.2 Spectrum of azimuthal decorrelation

The better consistency between generators in space-like variables such as pseudorapidity as suggested by Fig.4.3 has lead to the decision to investigate the aforementioned normalized azimuthal decorrelation $\frac{1}{\sigma}\frac{d\sigma}{d\Delta\phi}$.

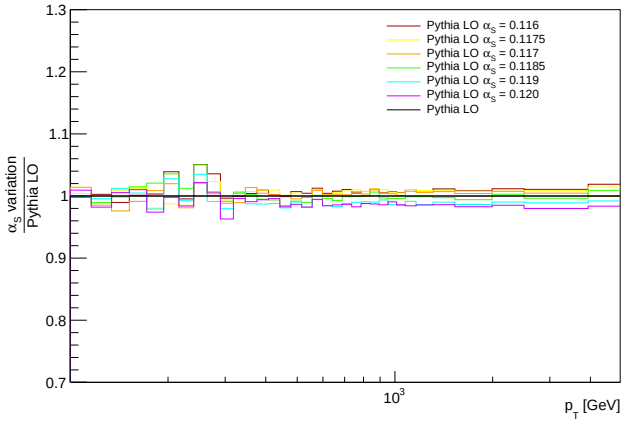

(a) Variation of α_S for Pythia

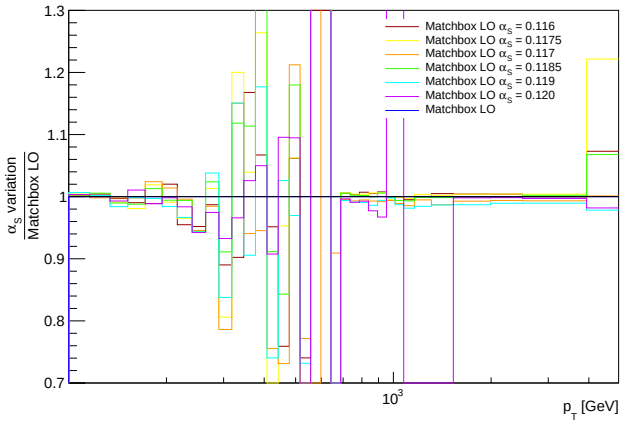

(b) Variation of α_S for Herwig

Fig. 4.2: The ratio plots demonstrating the effect of α_S variation on the shape of the spectrum within Herwig Matchbox LO and Pythia LO models for jets with $|y| < 4.8$ and $p_T > 100$ GeV.

This variable expresses the extent to which the leading dijet (the two jets with the highest p_T) is so called back to back. If there are only two jets in event, they should be fully back to back from the conservation of momentum and so their azimuthal decorrelation should be $\Delta\Phi = \pi$. If there is however another jet (comming from the same vertex) to be found then the $\Delta\phi$ could no longer be π unless the third jet were infinitely soft, which would then of course have no physical meaning. A sketch of the two situations just described is shown in Fig.4.4.

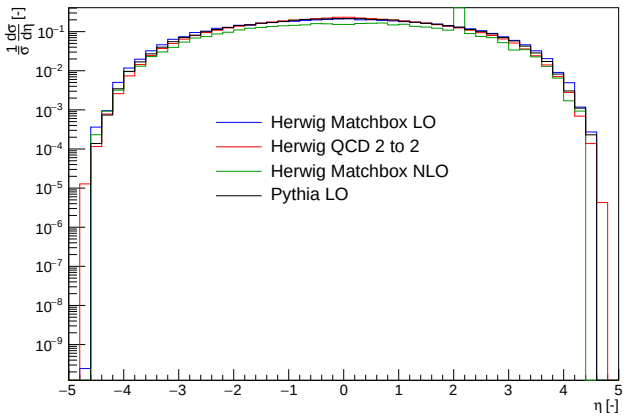

(a) value

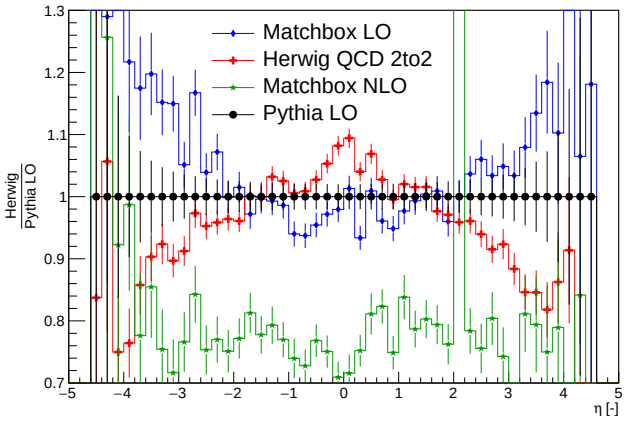

(b) ratios

Fig. 4.3: The spectrum of normalized pseudorapidity for different generator types and the ratio of their value vs. the value of Pythia LO. Spectra for jets with $p_T > 100$ GeV.

The emission of additional jet causes then the flattening of $\Delta\phi$ spectrum. If the Fig.4.5(a) is inspected then it is obvious that the naive image of one single peak at π is far from reality. That is because of the existence of jets comming from showering. It is however clearly visible that these effects decrease exponentially. Fig.4.5 do not show the entire range from zero, but only the region of $\Delta\phi \in (\frac{\pi}{2}, \pi)$. This is so because the effects of additional parton jet are the most pronounced in the region around $\frac{2}{3}\pi$ and therefore again the need arises to have the most precise and consistent description in this region. As can

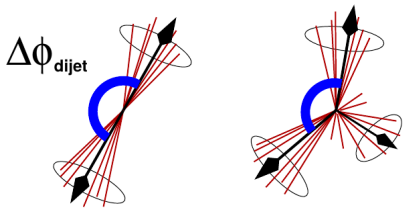

Fig. 4.4: The demonstration of the meaning of azimuthal decorrelation. [15]

be seen in 4.5(c) and (d), the influence of variation of α_S in generators is much lower than that of the different generators them selves. This is partly due to the merging procedures that has taken many jets out of the game and in polishing the p_T spectrum jeopardised the $\Delta\phi$ one. This could be either remedied by better merging procedure or higher statistics.

Fig.4.7 demonstrates the flattening of the peak at $\Delta\phi = \pi$, when the condition on having at least three jets per event is added. There is a clear plateau forming from $\Delta\phi \gtrsim 2.1$ in the Fig.4.7(a), that reflects the idea of decreasing azimuthal decorrelation through emission of additional jets. This plateau is there, due to the fact that all three jets never have the exactly same momentum and therefore their orientation in space is always at least a bit twisted from the exact equidistant orientation. It can be expected that this shift in $\Delta\phi$ would be more pronounced in the NLO, because in LO the only production mechanism for additional jets is from shower which is not as exclusively sensitive to α_S as desired.

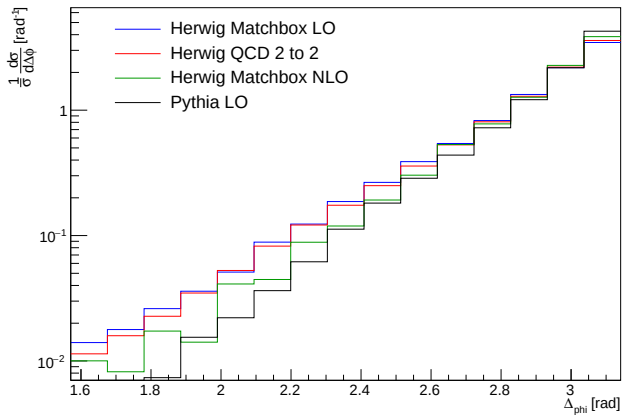

(a) Normalised spectrum

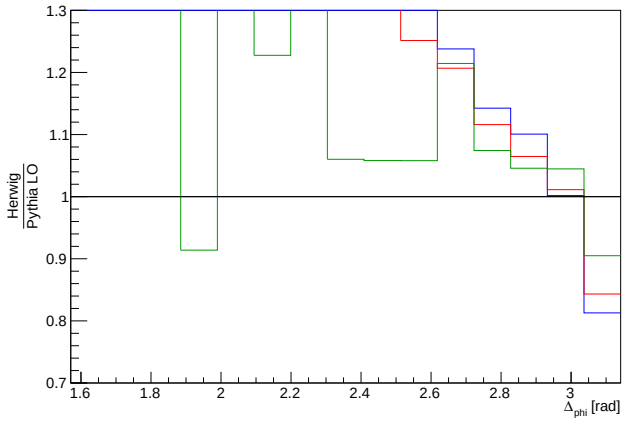

(b) Generator variations

Fig. 4.5: The spectrum of normalized azimuthal decorrelation of the two leading jets in event for different generator types and the ratio of their value vs. the value of Pythia LO. Spectra for jets with $|y| < 4.8$ and $p_T > 100$ GeV.

4.4 Future development

The future of this work is to try and eliminate the discrepancies between the generators by correcting the merging of data samples from different $\hat{p_T}$ bins. This will probably be best achieved by requesting official data set from ATLAS and a reference MC sample with correct official tune, where such effects as showering algorithm and hadronization scheme could be taken to be negligible. This could then be used as a new baseline to which the models used so far

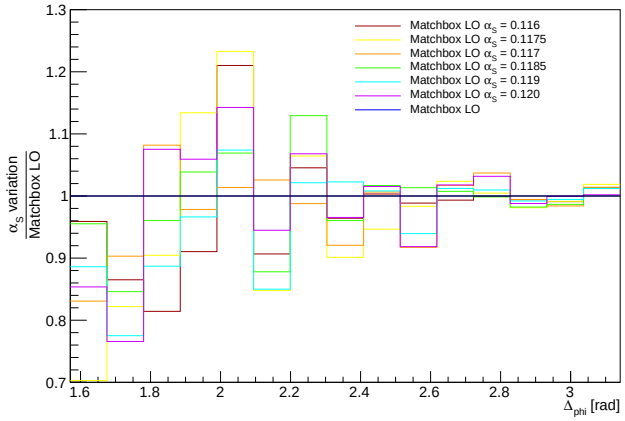

(a) Herwig α_S variations

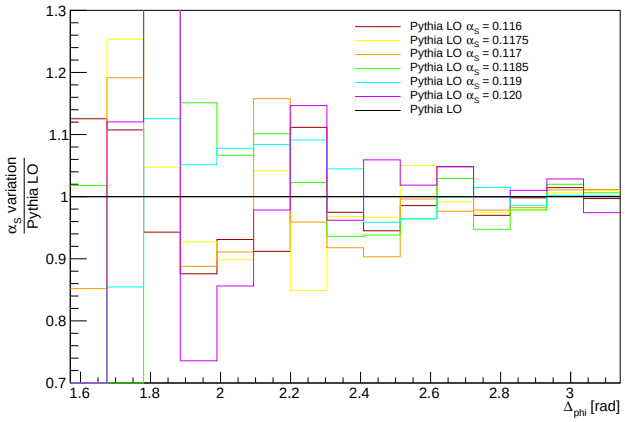

(b) Pythia α_S variations

Fig. 4.6: The effects of α_S variation on the shape of $\Delta\phi$ spectrum within Herwig Matchbox LO model**(a)** and Pythia LO**(b)**.

could be tuned. The tuned monte carlo models can be then theoretically used for generation of original data sets with different values of α_S which could then in turn yield information about the influence of these variations. In order to speed up the generation of the original data sets, more thorough research of the reweighting procedure mentioned above is one possible approach that could be very useful. Another future goal is to take into account the uncertainties stemming from PDF variations and try and minimise these.

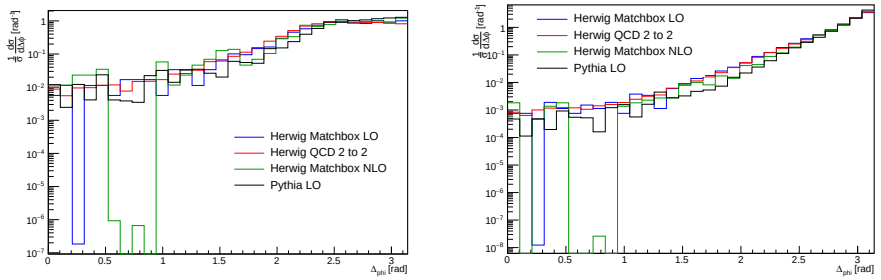

(a) At least three jets per event **(b)** At least two jets per event

Fig. 4.7: The comparison of spectra of normalized azimuthal decorrelation of the two leading jets in event for different generator types for event with at least three jets per event(a) and at least two jets per event(b). Spectra for jets with $|y| < 4.8$ and $p_T > 100$ GeV.

Chapter 5

Conclusion

The main theme of this thesis is the investigation of the possibility of measuring the value of strong coupling α_S from the jet kinematics at the ATLAS detector. Therefore we focus on four models simulating proton collisions and quantify the uncertainties from their predictions.

In order to better understand the physics motivation for this research, the thesis provides a brief overview of the standard model of particle physics in the first chapter, with the focus on the theory of quantum chromodynamics and the structure of proton in the second chapter. The third chapter reviews several possible methods of measuring the value of alpha S, such as the fitting of nucleon structure function and gluon distributions from electron-positron collisions, the examination of decay ratios of Z boson and τ leptons and the fitting of PDFs from proton-proton collisions.

This is followed by a chapter depicting the endeavour to test the influence of α_S on the shape of some kinematic variables against the influence of generator effects. The latter has proven to be the stronger so far, especially in case of p_T where the differences between the models are at their strongest. The generators in question were Pythia 8.2.3.5 with the PDF NNPDF23 tuned according to ATLAS A14 tune and three models implemented in Herwig 7 generator with the PDF MMHT2014. One with default LO matrix element QCD2to2 that is the part of Herwig 7 default equipment. And the other two models has been the Matchbox procedure in combination with MadGraph:OpenLoops package for matrix elements. Matchbox provides the matching of matrix element with showering procedure from Herwig in order to correctly merge the jet spectra from parton and shower. The Matchbox has been used in for LO and NLO matrix elements and showers. The most probable cause of discrepancies between the models have been identified as a possible error in merging different data samples during the generation of respective data sets. The evidence for this assumption is that the number and placement of the highest deviations agrees with that of the p_T ranges used during generation (see Appendix B). This must be remedied before continuing the endeavour to asses the theoretical uncertainties stemming from α_S variation within each model.

Future goals are then:

- Fixing the merging of data samples and correctly implementing the reweighting procedure for Matchbox models.
- Finding the correct tuning of all generators in order to minimise or ideally eliminate their influence.
- Assessing the uncertainty of $\Delta\phi$ spectra stemming from PDFs and take it into account during the analysis of the influence of α_S on the shape.
- Finding a reasonably fast way to generate NLO data for more precise measurements of α_S.
- Determining if the shape of $\Delta\phi$ spectrum in NLO can be used to measure the value of α_S.

Appendix A

Steering parameters of Pythia generator

```
PT samples for Pythia: [50 200 300 400 500 642 786 894 952 1076 1162 1310 1530 1992 2500 3137 393

Main:numberOfEvents = 1000000
PDF:pSet = LHAPDF6:NNPDF23_lo_as_0119_qed.LHgrid
Tune:pp=21
Beams:idA = 2212     ! first incoming beam is a 2212, a proton
Beams:idB = 2212     ! second beam is also a proton
Beams:eCM = 13000.   ! cm energy of collisions
HardQCD:all = on
PartonLevel:FSR = on
PartonLevel:ISR = on
PartonLevel:MPI = on
111:mayDecay = off        ! Do not decay pi0 -> shorter&faster outputs
Print:quiet = on
Random:setSeed = on

PhaseSpace:pTHatMin = pTHatMin
PhaseSpace:pTHatMax = pTHatMax

SigmaProcess:alphaSvalue = lphaS
TimeShower:alphaSvalue = alphaS
SpaceShower:alphaSvalue = alphaS
MultipartonInteractions:alphaSvalue = alphaS
```

Appendix B

Steering parameters of Herwig generator

B.1 QCD2to2

```
#PT range of samples: [40. 100. 200. 400. 800. 1600. 5000. 8000.]

read snippets/PPCollider.in

cd /Herwig/Generators

set EventGenerator:EventHandler:LuminosityFunction:Energy 13000.0

cd /Herwig/MatrixElements/

# QCD 2-2 scattering

insert SubProcess:MatrixElements[0] MEQCD2to2

set /Herwig/Cuts/JetKtCut:MinKT minkt*GeV
set /Herwig/Cuts/JetKtCut:MaxKT maxkt*GeV

cd /Herwig/Analysis
create Mira::Browser BrowserAnalysis Browser.so
insert /Herwig/Generators/EventGenerator:AnalysisHandlers 1 BrowserAnalysis

cd /Herwig/Generators
saverun LHC EventGenerator
```

B.2 Matchbox LO/NLO

```
PT samples of LO: [50. 650. 1000. 1500. 2000. 8000.]


read snippets/Matchbox.in
read snippets/PPCollider.in

cd /Herwig/EventHandlers
set EventHandler:LuminosityFunction:Energy 13000*GeV

read Matchbox/StandardModelLike.in
read Matchbox/DiagonalCKM.in

cd /Herwig/MatrixElements/Matchbox
set Factory:OrderInAlphaS 2
set Factory:OrderInAlphaEW 0

set /Herwig/Couplings/NLOAlphaS:input_scale 91.1876*GeV
set /Herwig/Couplings/NLOAlphaS:input_alpha_s alphaS
set /Herwig/Model:QCD/RunningAlphaS /Herwig/Couplings/NLOAlphaS

do Factory:Process p p -> j j

set /Herwig/UnderlyingEvent/MPIHandler:IdenticalToUE 0

read Matchbox/MadGraph-OpenLoops.in
cd /Herwig/MatrixElements/Matchbox
set Factory:ScaleChoice Scales/MaxJetPtScale

cd /Herwig/Cuts
set Cuts:JetFinder JetFinder
insert Cuts:MultiCuts 0 JetCuts
insert JetCuts:JetRegions 0 FirstJet
cd /Herwig/Cuts
set FirstJet:PtMin @minkt@*GeV
set FirstJet:PtMax @maxkt@*GeV
do FirstJet:YRange -5. 5.0

set JetFinder:Variant AntiKt
set JetFinder:ConeRadius 0.4

## LO
read Matchbox/LO-DefaultShower.in
```

```
## NLO
#read Matchbox/MCatNLO-DefaultShower.in

read Matchbox/FiveFlavourScheme.in
read Matchbox/MMHT2014.in

cd /Herwig/Analysis
create Mira::Browser BrowserAnalysis Browser.so
insert /Herwig/Generators/EventGenerator:AnalysisHandlers 1 BrowserAnalysis

do /Herwig/MatrixElements/Matchbox/Factory:ProductionMode

cd /Herwig/Generators
saverun LHC-Matchbox-LO EventGenerator
```

Bibliography

[1] *ATLAS Run 1 Pythia8 tunes*, Tech. Rep. ATL-PHYS-PUB-2014-021, CERN, Geneva, Nov 2014.

[2] G. Aad et al., *Measurement of the $t\bar{t}$ production cross-section using $e\mu$ events with b-tagged jets in pp collisions at $\sqrt{s}$ = 7 and 8* TeV *with the ATLAS detector*, Eur. Phys. J., C74 (2014), p. 3109. [Addendum: Eur. Phys. J.C76,no.11,642(2016)].

[3] R. Aaij et al., *Observation of the resonant character of the $Z(4430)^-$ state*, Phys. Rev. Lett., 112 (2014), p. 222002.

[4] ——, *Observation of $J/\psi p$ Resonances Consistent with Pentaquark States in $\Lambda_b^0 \to J/\psi K^- p$ Decays*, Phys. Rev. Lett., 115 (2015), p. 072001.

[5] C. Anastasiou, C. Duhr, F. Dulat, E. Furlan, T. Gehrmann, F. Herzog, A. Lazopoulos, and B. Mistlberger, *High precision determination of the gluon fusion Higgs boson cross-section at the LHC*, JHEP, 05 (2016), p. 058.

[6] J. Bellm et al., *Herwig 7.0/Herwig++ 3.0 release note*, Eur. Phys. J., C76 (2016), p. 196.

[7] J. Bellm, S. Gieseke, and S. Plätzer, *Merging NLO Multi-jet Calculations with Improved Unitarization*, Eur. Phys. J., C78 (2018), p. 244.

[8] P. Bolzoni, B. A. Kniehl, and A. V. Kotikov, *Average gluon and quark jet multiplicities at higher orders*, Nucl. Phys., B875 (2013), pp. 18–44.

[9] E. Braaten, S. Narison, and A. Pich, *QCD analysis of the tau hadronic width*, Nucl. Phys., B373 (1992), pp. 581–612.

[10] M. Cacciari, G. P. Salam, and G. Soyez, *FastJet User Manual*, Eur. Phys. J., C72 (2012), p. 1896.

[11] C. Collaboration, *Measurements of inclusive 2-jet, 3-jet and 4-jet azimuthal correlations in pp collisions at $\sqrt{s} = 13$* TeV, (2017).

[12] A. Deur, S. J. Brodsky, and G. F. de Teramond, *The QCD Running Coupling*, Prog. Part. Nucl. Phys., 90 (2016), pp. 1–74.

[13] R. P. Feynman, *Very high-energy collisions of hadrons*, Phys. Rev. Lett., 23 (1969), pp. 1415–1417. [,494(1969)].

[14] J. I. Friedman and H. W. Kendall, *Deep inelastic electron scattering*, Ann. Rev. Nucl. Part. Sci., 22 (1972), pp. 203–254.

[15] O. Kepka, *The qcd analysis of multijet events in proton-antiproton collisions at the tevatron*, Master's thesis, MFF UK in Prague, 2006.

[16] V. Khachatryan et al., *Measurement of dijet azimuthal decorrelation in pp collisions at* $\sqrt{s} = 8\,\text{TeV}$, Eur. Phys. J., C76 (2016), p. 536.

[17] B. Malaescu and P. Starovoitov, *Evaluation of the Strong Coupling Constant* α_S *Using the ATLAS Inclusive Jet Cross-Section Data*, Eur. Phys. J., C72 (2012), p. 2041.

[18] K. A. Olive et al., *Review of Particle Physics*, Chin. Phys., C38 (2014), p. 090001.

[19] C. Patrignani et al., *Review of Particle Physics*, Chin. Phys., C40 (2016), p. 100001.

[20] C. Quigg, *Gauge Theories of the Strong, Weak, and Electromagnetic Interactions*, Princeton University Press, USA, 2013.

[21] G. P. Salam, *The strong coupling: a theoretical perspective*, 2017.

[22] T. Sjostrand, S. Mrenna, and P. Z. Skands, *PYTHIA 6.4 Physics and Manual*, JHEP, 05 (2006), p. 026.

[23] Wikipedia.org, *Standard model of elementary particles*, (2008).